PAPER

Check for updates

A gold nanobipyramid-based photothermal reagent with functions of targeting and activatable fluorescence labeling for visual photothermal therapy†

Xueke Wu,‡[ab] Chenyuan Yan,‡[ab] Lixuan Mu, [iD] *[a] Yuan Wang,[ab] Guangwei She [iD] [a] and Wensheng Shi*[abc]

By assembling fluorophore-marked DNA stem-loops on the surface of gold nanobipyramids (AuNBPs) with an efficient photothermal conversion, we fabricated a multifunctional photothermal reagent (AuNBPs-mPEG/AA-TR). The sgc8 sequences that were embedded inside the DNA stem-loops can specifically target the PTK7, an overexpressed protein located on the surface of CCRF-CEM cells (human acute lymphoblastic leukemia T lymphocyte) to realize an active targeting function. Before the AuNBPs-mPEG/AA-TR bind to the PTK7 proteins, the DNA stem-loops are folded, and the fluorophore linked on the DNA stem-loop will be close to the AuNBPs. In this configuration, the fluorescence from the fluorophore is quenched by the AuNBPs. However, when the AuNBPs-mPEG/AA-TR bound to the PTK7 proteins through the sgc8 sequences, the DNA stem-loops can be opened partially to enable the fluorophore to be far away from the AuNBPs. As a result, the fluorescent signal will be activated. Therefore, the fluorescence can be used as a visual signal to reveal the binding between the AuNBPs-mPEG/AA-TR and CCRF-CEM cells (usually called activatable fluorescence labelling). While under irradiation of an 808 nm laser, the CCRF-CEM cells could be ablated through the photothermal therapy of the AuNBPs-mPEG/AA-TR with a high photothermal efficiency. Applying the AuNBPs-mPEG/AA-TR to Human B lymphoma cells (Ramos cells) and CCRF-CEM cells, we found that only the CCRF-CEM cells can be effectively targeted, actively fluorescently labeled, and readily ablated by the AuNBPs-mPEG/AA-TR. This work provides an alternative photothermal agent for the targeted therapy of tumors.

Introduction

Photothermal therapy (PTT) can ablate cancer cells with a small invasion and short treatment time.[1,2] In this process, the energy of infrared light can be transformed into heat energy by a photothermal reagent to directly kill cancer cells. Among various photothermal reagents, gold nanomaterials such as gold nanorod (AuNRs), *etc.* have received much attention due to their tunable localized surface plasma resonance (LSPR) peak, favorable biocompatibility, and excellent photothermal conversion ability.[3–5] In addition to these advantages, gold

nanobipyramids (AuNBPs) as a novel gold nanostructure have a higher photothermal conversion efficiency than AuNRs at the same LSPR peak.[6–8] Moreover, two distinctive tips of the AuNBPs can produce a stronger electric field, by which the fluorescence, absorption and Raman signals of a probe can be significantly enhanced.[9–11] Therefore, AuNBPs and the corresponding nano-composite have been incorporated in PTT. Recently, AuNBPs were loaded onto black phosphorus nanosheets for PTT of deep-seated orthotopic lung tumors.[12] In another example, the polydopamine–AuNBPs composite also exhibited superior photothermal properties in PTT.[13] However, AuNBPs used as a photothermal reagent were always passively concentrated toward tumors through the enhanced permeability and retention effect (EPR). In this way, the final distribution of the AuNBPs in the tumor would be often unsatisfactory and the final therapy will inevitably suffer from a major setback due to the off-target of the photothermal reagent during the PTT.[14] In order to overcome this shortcoming of AuNBPs, targeting is a promising alternative, in which the apta-mers, antibodies, or polypeptides used as biomarker-targeting ligands were modified onto the photothermal reagent of the

[a] *Key Laboratory of Photochemical Conversion and Optoelectronic Materials, Technical Institute of Physics and Chemistry, Chinese Academy of Sciences, Beijing 100190, China. E-mail: mulixuan@mail.ipc.ac.cn, shiws@mail.ipc.ac.cn*

[b] *University of Chinese Academy of Sciences, Beijing 100049, China*

[c] *Ganjiang Innovation Academy, Chinese Academy of Sciences, Ganzhou 341000, China*

† Electronic supplementary information (ESI) available. See DOI: https://doi.org/10.1039/d2ma00456a

‡ Both authors contributed equally to this work.

AuNBPs to identify tumor sites[15,16] and further promote the uptake by the cells.[17] Among these ligands, aptamers possess a simple composition, small size and stable structure, moreover, they could readily bind to the proteins and cells with high affinity and specificity. For example, the aptamer of a sgc8 sequence can specifically bind to protein tyrosine kinase 7 (PTK7),[18] a tumor marker that is overexpressed on the surface of the CCRF-CEM (human acute lymphoblastic leukemia T lymphocyte).[19–21] The sgc8 sequence has been used to modify black phosphorus for the targeted photothermal therapy of the CCRF-CEM.[22] Furthermore, one end of the sgc8 sequence can also be marked by a fluorophore such as Texas red (TR) to fluorescently label cells, by which the cancerous cells can be lightened for the convenience of clinical therapy. However, a disadvantage of this strategy should be considered. The photothermal reagent marked by the fluorophore still emits fluorescence even when it is not targeted toward cancerous cells, which would cause a strong fluorescence background during the diagnosis. As a result, the resolution for differentiating cancerous cells from normal ones would be unsatisfactory for clinicians.[23–25] Considering the excellent photothermal conversion efficiency of AuNBPs and the benefits of the targeting strategy as well as the problem with the fluorophore label, in this work, we together assembled a DNA stem loop containing the TR-marked sgc8 sequence (AA-TR) and polyethylene glycol (mPEG) onto the surface of AuNBPs, and a multifunctional photothermal reagent (AuNBPs-mPEG/AA-TR) was achieved. In this way, not only can targeting and fluorescence labelling be realized during photothermal therapy with a high conversion efficiency, but also the fluorescence of the reagent can only be triggered by the interaction between the reagent and the cancerous cells. As shown in Scheme 1, the AA-TR on the surface of the AuNBPs is in closed form before the AuNBPs-mPEG/AA-TR was targeted to the CCRF-CEM cell. In this state, the fluorescence of the TR is quenched by the AuNBPs due to the energy transfer from the TR to the AuNBPs. However, the stem-loop structure of the AA-TR can be opened partially when the sgc8 is specifically targeted toward the PTK7 on the surface of the CCRF-CEM cells. As a result, the TR would leave the AuNBPs and the energy transfer from the TR to AuNBPs would be inhibited partially. Thus, the TR fluorescence previously quenched by the AuNBPs would be recovered. Clearly, it is the binding between the sgc8 and PTK7 that triggers the TR fluorescence. Therefore, the TR fluorescence would reveal the target of the AuNBPs-mPEG/AA-TR to CCRF-CEM cells and can be utilized to assist a clinician to visually monitor the interaction between the photothermal reagent and cancer cells and differentiate between the normal and cancerous cells. Moreover, modification of the mPEG on the surface of the AuNBPs could improve the dispersion stability of the photothermal reagent in medium. Applying the photothermal reagent developed in this work to the CCRF-CEM cells and Romas cells, we found that the AuNBPs-mPEG/AA-TR exhibits targeting and activatable fluorescence labelling only toward the CCRF-CEM cells, and only the CCRF-CEM cells can be effectively ablated by the irradiation of the 808 nm laser. This work provides a promising photothermal agent for targeted cancer therapies.
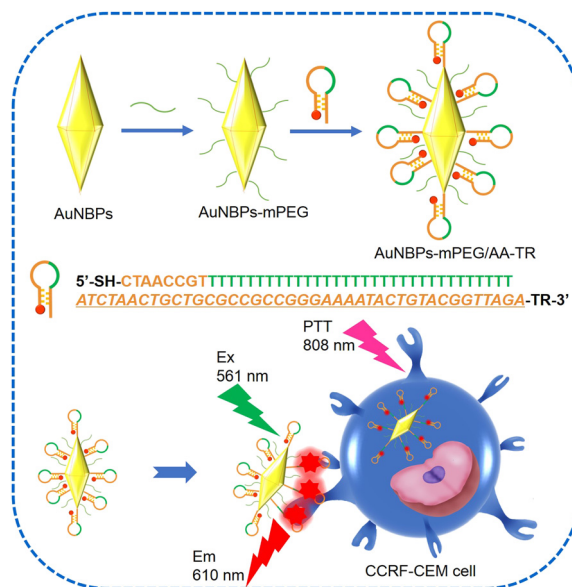
Scheme 1 Illustration of the AuNBPs-mPEG/AA-TR fabrication process and the schematic representation of AuNBPs-mPEG/AA-TR toward CCRF-CEM cells for PTT. The aptamer of sgc8 is in italic type.

Experimental

Materials and reagents

All reagents in this work were used without further purification or treatment. Gold chloride trihydrate ($HAuCl_4 \cdot 3H_2O$), sulphydryl polyethylene glycol (mPEG, 2000), cetyltrimethylammonium bromide (CTAB), cetyltrimethylammonium chloride (CTAC), tris–carboxyethylphosphine (TCEP), and sodium borohydride ($NaBH_4$) were purchased from Aladdin (Shanghai, China). Ascorbic acid (AA), ammonia solution ($NH_3 \cdot H_2O$, 25%), hydrochloric acid (HCl), hydrogen peroxide (H_2O_2, 30%), sodium citrate, and sodium chloride (NaCl) were all purchased from Beijing Chemical Reagent Company (Beijing, China). Tris–Ethylenediaminetetraacetic acid (EDTA) buffer solution (pH = 8.0) and phosphate buffered saline (PBS, Na_2HPO_4 10 mmol L^{-1}, KH_2PO_4 2 mmol L^{-1}, NaCl 137 mmol L^{-1}, KCl 2.7 mmol L^{-1}, pH = 7.4) were obtained from Solarbio Science & Technology (Beijing, China). Hoechst 33342 was purchased from Biodee Biotechnology (Beijing, China). Calcein AM and propidium iodide (PI) were purchased from Sigma (Shanghai, China). The DNA sequences used in the experiment are listed in Table S1, ESI,† and were ordered from Sangon Biotech (Shanghai, China).

Apparatus

The instruments used in the experiment are as follows: a centrifuge (H2050R), transmission electron microscopes (TEM, HT7700), a fluorescence spectrometer (HITACHI, F4600), an ultraviolet-visible spectrophotometer (HITACHI, U-3900), a nanometer particle size and zeta potential analyser (Zetasizer Nano ZS) and a confocal laser scanning microscope (Nikon A1).

Synthesis of the AuNBPs

The LSPR peak of AuNBPs used in this work is located at 750 nm. The specific preparation method refer to our previous work,[7] and 2.5 mL of seed solution was selected in this work.

Synthesis of the AuNBPs-mPEG/AA-TR

mPEG (10–50 μL, 2 mM) was added to 2 mL of AuNBP solution (90 μg mL^{-1}). The mixing solution was stirred overnight and centrifuged. The product was washed with pure water and redispersed in 1 mL of water to obtain the AuNBPs-mPEG solution.

10 μL of HCl (1 N) and 10 μL of SDS (1%) were added to AuNBPs-mPEG solution. The mixing solution was stirred for 30 minutes. Then, the AA-TR (100 μM, 20 μL) activated by TCEP in acetate buffer (pH = 5.2) was added to the mixing solution. After the mixing solution was stirred overnight, 10 μL of NaCl solution (2 M) was added to it every half hour until the concentration of NaCl in the mixing solution reached 0.1 M. After 12 h, the mixing solution was centrifuged and the precipitate was washed with ultrapure water until the supernatant had no fluorescence. Finally, the product named AuNBPs-mPEG/AA-TR was dispersed in 1 mL of PBS (0.01 M) solution for further tests.

Cytotoxicity assay

Firstly, CCRF-CEM cells were inoculated into three 96-well plates, and the inoculation density of each well was 7×10^3 cells. After 12 h, AuNBPs, AuNBPs-mPEG and AuNBPs-mPEG/AA-TR with different concentrations were added to each well of the 96-well plates respectively, and co-cultured with CCRF-CEM cells for 24 h. Then the medium was removed, and 0.1 mL of MTT (0.5 mg mL^{-1} in RPMI medium 1640) was added to each well, followed by incubation for 4 h at 37 °C. Finally, 110 μL of DMSO is added to each well. The absorbance values of each well were collected at 490 nm.

Confocal laser scanning microscopy (CLSM) observation

AuNBPs-mPEG/AA-TR (10 μL, 150 μg mL^{-1}) were co-cultured with CCRF-CEM cells (1.5 mL) and Roman cells (1.5 mL) in a confocal culture dish for 2 h, respectively. Hoechst 33342 was then used to stain the nucleus of the two kinds of cells (1 mg mL^{-1}, 10 μL) for 10 minutes. The 405 and 561 nm lasers were used as excitation sources for the Hoechst 33342 and AuNBPs-mPEG/AA-TR, respectively.

Live/dead cell (CCRF-CEM) assay

CCRF-CEM cells were inoculated into 24-well plates with an 8×10^3 inoculation density. The CCRF-CEM cells was divided into two groups, and each group had four samples. Equal amounts of the AuNBPs-mPEG/AA-TR (60 μg mL^{-1}, 30 μL) were added ot each sample of the second group. After 2 h, all samples were irradiated by an 808 nm laser with different powers for 10 min, and then a mixture of 10 μL calcein AM and PI (10 μM, v/v = 1 : 2) was added to each well to label the survival status of the cells. A 488 nm laser was used as the co-excitation source of calcein AM and PI.

Results and discussion

Charaterization of structure and photothermal properties

The TEM image of the AuNBPs is shown in Fig. 1a. The size of the AuNBPs is quite uniform with a length of about 65 nm and a width of about 23 nm. The longitudinal plasma resonance wavelength (LPRW) of the AuNBPs is around 750 nm determined from the UV-vis absorption spectrum (Fig. 1b).

The photothermal conversion of the AuNBPs was investigated. The aqueous solutions with a volume of 1 mL and various concentrations of AuNBPs (0, 5, 15, and 30 μg mL^{-1}) were separately irradiated using an 808 nm laser (1.0 W cm^{-2}). Meanwhile, the temperatures of the solutions were monitored using a thermocouple. As shown in Fig. 2a, the temperature of the solutions containing the AuNBPs was gradually enhanced with the continuation of the irradiation, while the temperature of the solution without the AuNBPs only showed a slight change. Over the same duration, the higher the concentration of the AuNPBs was, the more significant the change of temperature was. After irradiation for 10 min, the temperature of the solution containing the AuNBPs of 30 μg mL^{-1} can increase by about 25 °C. Under a different power density of laser irradiation, the photothermal temperature change of solution was also investigated (Fig. S1, ESI†). Furthermore, the photothermal stability of the AuNBPs was evaluated. After five cycles between "laser on" and "laser off" states (Fig. 2b), the AuNBPs still exhibited a strong photothermal conversion. These results
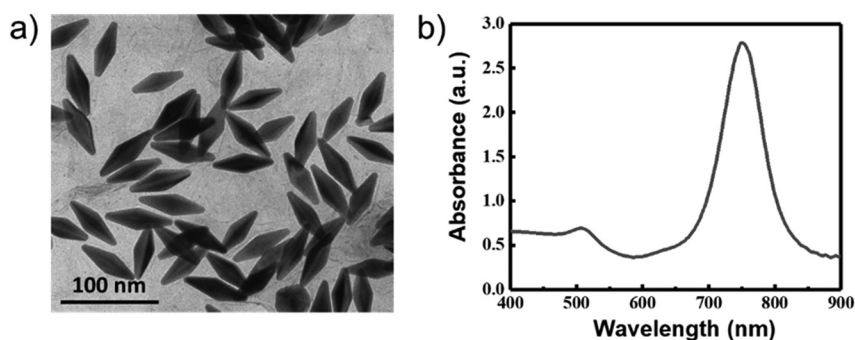

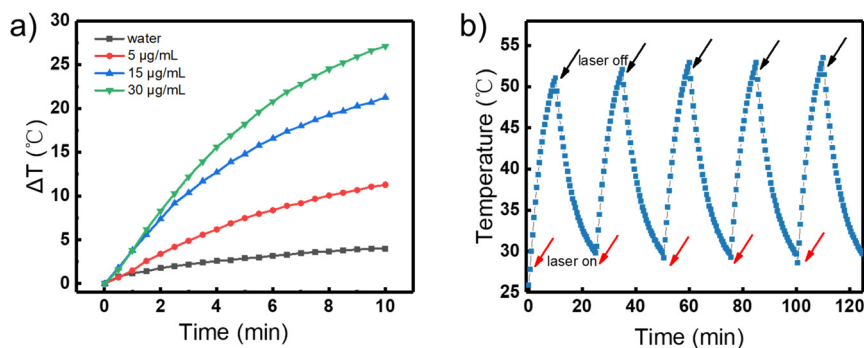Fig. 1 (a) TEM and (b) UV-Vis absorption spectrum of the AuNBPs.

Fig. 2 (a) Temperature dependences of aqueous solution with various concentrations of the AuNBPs on the irradiation time of 808 nm lasers (1.0 W cm^{-2}). (b) Photothermal stability of the AuNBPs (30 µg mL^{-1}, 1 mL; laser: 808 nm, 1.0 W cm^{-2}).

indicated that the AuNBPs have a high and stable photothermal conversion and potential for the construction of novel photothermal reagents.

To improve the biocompatibility and dispersion stability of the reagents in aqueous solution, mPEG was previously modified onto the surface of the AuNBPs through the interaction between the AuNBPs and the –SH of the mPEG, and then the mPEG-modified AuNBPs was decorated with the AA-TR to obtain the AuNBPs-mPEG/AA-TR. Using the fluorescence intensity of the AuNBPs-mPEG/AA-TR as a criterion, we optimized the concentration of the mPEG added in the reaction system under a fixed concentration of the AA-TR, and the results are shown in Fig. S2 (ESI†). With the increase in the concentration of mPEG, the fluorescence intensity of the AuNBPs-mPEG/AA-TR was enhanced gradually and reached a maximum at 30 µM of the mPEG, then decreased gradually with the further increase in mPEG. When the concentration of the mPEG is low, only a small amount of mPEG can be modified onto the surface of the AuNBPs. Too little mPEG on the AuNBPs is not enough to improve the dispersion stability of the AuNPBs-mPEG/AA-TR in solution. As a result, the AuNPBs-mPEG/AA-TR would aggregate and settle, and only weak fluorescence can be detected from the suspending reagents. However, when the concentration of mPEG is too high, the excess mPEG would occupy the numerous sites of the AuNBPs surface in advance, which would block the subsequent modification of the AA-TR. Therefore, only low fluorescence intensity can be detected at a high concentration of mPEG. 30 µM of mPEG is an optimal concentration, and was chosen in the later preparation of the AuNBPs-mPEG/AA-TR. Moreover, the dispersion stabilities of the AuNBPs-mPEG/AA-TR and AuNBPs-AA-TR (without mPEG) were compared. Fig. S3 (ESI†) shows the photographs of the freshly prepared AuNBPs-AA-TR and AuNBPs-mPEG/AA-TR as well as that standing for 72 h. A small amount of precipitate can be observed from the AuNBPs-AA-TR standing for 72 h (Fig. S3a-1 and b-1, ESI†). However, the precipitate cannot be found from the AuNBPs-mPEG/AA-TR even after standing for 72 h (Fig. S3a-2 and b-2, ESI†), indicating that the dispersion stability of the reagents can be significantly improved through the optimal modification of the mPEG on the surface of AuNBPs.

To characterize the assembly of the AA-TR and mPEG on the surface of the AuNBPs, we investigated the potential changes of the reagents using a zeta potentiometer after each step of the modification, and the results are shown in Fig. S4a (ESI†). The AuNBPs freshly prepared exhibited a positive zeta potential (+32.5 mV) due to the presence of the CTAB around the surface of the AuNBPs. However, the AuNBPs-mPEG has a positive zeta potential (+18 mV). The decrease of zeta potential is a result of a part replacement of the positive CTAB by the neutral mPEG. Furthermore, the zeta potential of the AuNBPs-mPEG/AA-TR was negative, which can be ascribed to further modification of the AA-TR that has a large number of negative PO$_4^{3-}$. The change of the zeta potential from +32.5 mV to +18 mV and finally to a negative one indicated that the mPEG and AA-TR were successfully assembled step by step onto the surface of the AuNBPs to form the AuNBPs-mPEG and AuNBPs-mPEG/AA-TR, respectively. The absorption spectra of the AuNBPs, AuNBPs-mPEG and AuNBPs-mPEG/AA-TR were investigated. As shown in Fig. S4b (ESI†), the longitudinal plasmonic peaks of the AuNBPs-mPEG and AuNBPs-mPEG/AA-TR were slightly red-shifted compared with that of the AuNBPs, which resulted from a change in the refractive index of the AuNBPs surface after these modifications.[26] These results further demonstrated that the modifications of the mPEG and AA-TR on the surface of the AuNBPs were successful.

To investigate the photothermal conversion efficiency of the AuNBPs-mPEG/AA-TR, the temperature of the solution containing the AuNBPs-mPEG/AA-TR was monitored during irradiation with the 808 nm laser (1.0 W cm^{-2}). After irradiation for 10 min, the light source was removed, and the temperature of the solutions was continuously recorded with a thermocouple for 15 min to obtain the temperature trace of the solution (Fig. 3). Based on Fig. 3, the photothermal conversion efficiency of the AuNBPs-mPEG/AA-TR was calculated to be 45.5%. Through the same method, the photothermal conversion efficiency of the AuNBPs was determined to be 51.1% according to the first cycle in Fig. 2b, indicating that the decoration of the AA-TR and mPEG on the surface of AuNBPs has a slight influence on the photothermal conversion of the AuNBPs.

The cytotoxicity of AuNBPs-mPEG/AA-TR

Furthermore, the cytotoxicity of the AuNBPs, AuNBPs-mPEG, and AuNBPs-mPEG/AA-TR was evaluated using the MTT method, and the results are shown in Fig. 4. The cytotoxicities
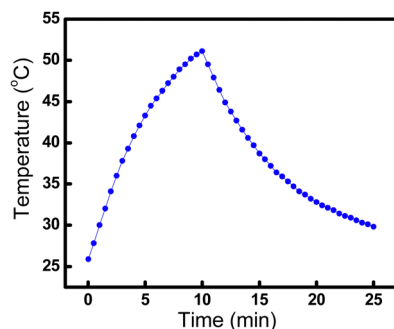
Fig. 3 Temperature curve of AuNBPs–mPEG/AA-TR (30 μg mL^{-1}, 1 mL). An 808 nm laser (1.0 W cm^{-2}) is used for the first 10 min, then the laser is turned off.
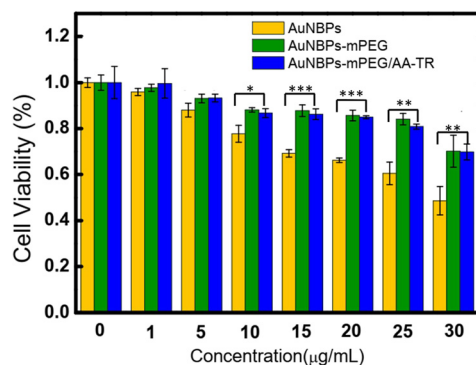

Fig. 4 Viability of CCRF-CEM cells after being incubated with AuNBPs, AuNBPs-mPEG and AuNBPs-mPEG/AA-TR for 24 h. ***: $P < 0.001$, **: $P < 0.01$, *: $P < 0.05$. All error bars represent the standard deviation determined from three independent assays.

of the AuNBPs-mPEG and AuNBPs-mPEG/AA-TR are similar and significantly less than those of the AuNBPs, indicating that the modification of the mPEG on the AuNBPs can indeed reduce the cytotoxicity of the reagents. Moreover, cell viability can be over 85% even when the concentration of the AuNBPs-mPEG/AA-TR reached 20 μg mL^{-1}, verifying that the AuNBPs-mPEG/AA-TR with a concentration less than 20 μg mL^{-1} is biocompatible. The cytotoxicity of AuNBPs-mPEG/AA-TR toward normal cells was also investigated and the results are shown in Fig. S5 (ESI†).

The targeting function of AuNBPs-mPEG/AA-TR

It is known that the targeting of the photothermal reagent toward cells is very crucial for PTT. Thus, the specific binding of the AuNBPs-mPEG/AA-TR to the CCRF-CEM cells was evaluated using flow cytometry, and the results are shown in Fig. 5. It can be observed that the intact CCRF-CEM cells only have a weak fluorescence (Fig. 5a-1), while the CCRF-CEM cells incubated with the AuNBPs-mPEG/AA-TR exhibited an enhancement in the fluorescence no matter the number of T bases used in the AA-TR was 16, 32 or 40 (Fig. 5a-3,4,5). However, no significant change in the fluorescence can be observed from a similar experiment with Ramos cells as the negative control (Fig. 5b-1,3,4,5). Accordingly, it can be demonstrated that the
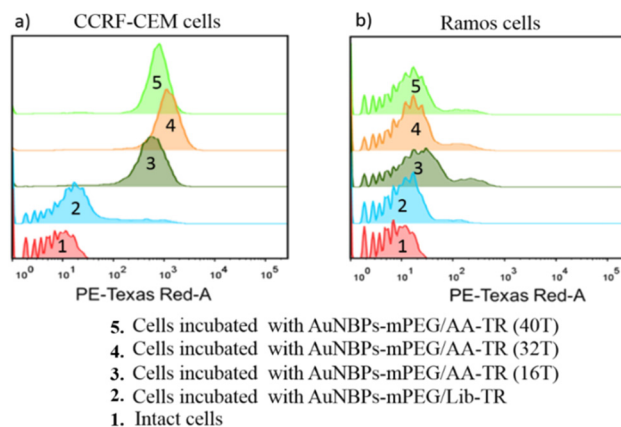

5. Cells incubated with AuNBPs-mPEG/AA-TR (40T)
4. Cells incubated with AuNBPs-mPEG/AA-TR (32T)
3. Cells incubated with AuNBPs-mPEG/AA-TR (16T)
2. Cells incubated with AuNBPs-mPEG/Lib-TR
1. Intact cells

Fig. 5 Flow cytometry analysis of the cells incubated with AuNBPs-mPEG/AA (nT, n = 16, 32, 40)-TR and AuNBPs-mPEG/Lib-TR: (a) CCRF-CEM and (b) Ramos.

AuNBPs-mPEG/AA-TR can specially target the CCRF-CEM cells. Furthermore, when the number of T bases in the AA-TR is 32, the CCRF-CEM cells incubated with the AuNBPs-mPEG/AA-TR exhibited the strongest fluorescence as shown in Fig. 5a-3,4,5. Therefore, the AA-TR with 32 T bases as an optimal structure were used in all of the AuNBPs-mPEG/AA-TRs in this work. To further verify that the targeting function was a result of the interaction between the aptamer (sgc8 sequence) and the PTK7 protein on the surface of the CCRF-CEM cell, a random DNA sequence (Lib) was used to replace the sgc8 sequence in the AA-TR to form the control sample of the AuNBPs-mPEG/Lib-TR. The fluorescence of the CCRF-CEM cells incubated with the AuNBPs-mPEG/Lib-TR is similar to that of the intact cells (Fig. 5a-2), revealing that the AuNBPs-mPEG/Lib-TR with the random DNA sequence of Lib can't bind to the CCRF-CEM cells. Clearly, it is the sgc8 sequence in AA-TR to produce the ability of targeting the AuNBPs-mPEG/AA-TR toward the CCRF-CEM cells. In order to more clearly observe the specific binding between the AuNBPs-mPEG/AA-TR and CCRF-CEM cells, the AuNBPs-mPEG/AA-TR was co-cultured with CCRF-CEM cells and Ramos cells, respectively. Meanwhile, the nuclei of the two kinds of cells were labeled by the Hoechst 33342. The fluorescence images of the cells were collected using a confocal imaging system and are shown in Fig. S6 (ESI†). Red fluorescence from the AuNBPs-mPEG/AA-TR and blue fluorescence from Hoechst 33342 were observed from the CCRF-CEM cells (Fig. S6a, ESI†). However, only blue fluorescence from Hoechst 33342 can be detected from the Ramos cells (Fig. S6b, ESI†), indicating that the AuNBPs-mPEG/AA-TR can't be bound to the Ramos cells. Therefore, these results demonstrated that the AuNBPs-mPEG/AA-TR are more inclined to bind to the CCRF-CEM cells rather than the Ramos cells under the same culture conditions, consistent with observations from the flow cytometry analysis.

The activatable fluorescence labelling function of AuNBPs-mPEG/AA-TR

To verify the activation of the fluorescence by the binding between the AuNBPs-mPEG/AA-TR and the CCRF-CEM cells, the AuNBPs-
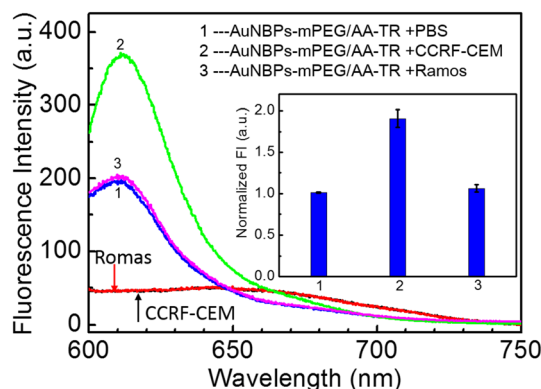
Fig. 6 Fluorescence spectra and normalized fluorescence intensity (inset: repeated three times in parallel) of AuNBPs-mPEG/AA-TR (same mass) after incubation with different medium (1. PBS, 2. CCRF-CEM cells, 3. Romas cells) for 2 h respectively.

mPEG/AA-TR with same quantity were dispersed into the cell culture mediums with the CCRF-CEM, Romas or PBS. Fluorescence spectra of three mixing solutions were acquired after incubation for 2 h, and the results are shown in Fig. 6. Obviously, the fluorescence intensity of the AuNBPs-mPEG/AA-TR in the culture medium with the CCRF-CEM cells was stronger at 610 nm than that in the culture medium with the Ramos cells or only PBS, and the former is almost double that of the latter (Fig. 6, inset). These results indicated that the fluorescence of the AuNBPs-mPEG/AA-TR could be activated by the combination of the reagent and the CCRF-CEM cells, which can be attributed to the special binding between the sgc8 sequence in AA-TR and the PTK7 protein on the surface of the cells.

The photothermal treatment function of AuNBPs-mPEG/AA-TR

The photothermal treatment of the AuNBPs-mPEG/AA-TR toward the CCRF-CEM cells was evaluated by the method of live/dead cell assay. The CCRF-CEM cells were divided into two groups, and each group has four samples. The samples in the first group (defined as only the laser group) did not contain the AuNBPs-mPEG/AA-TR. On the other hand, an equal amount of the AuNBPs-mPEG/AA-TR (60 μg mL^{-1}, 30 μL) was added in each sample of the second group (defined as laser + AuNBPs-mPEG/AA-TR group). After the incubation for 2 h, all samples in the two groups were irradiated with an 808 nm laser with various powers for 10 min. After the irradiation, calcein AM with green fluorescence and PI with red fluorescence were used to label living and dead cells, respectively. The survival status of the CCRF-CEM cells was observed using a fluorescence confocal microscope, and the results are shown in Fig. 7. Observing the first group, we can determine that all cells in the four samples only emitted green fluorescence even under the irradiation of 1.5 W cm^{-2}, indicating that the CCRF-CEM cells in the first group were live after the laser irradiation even at the power of 1.5 W cm^{-2} for 10 min. However, in the second group, the fluorescence of the cells gradually transformed from green to orange and red with the increase of the laser power. When the laser power was 0.5 W cm^{-2}, a small number of cells emitted orange and red fluorescence. As the laser power was increased to 1 W cm^{-2}, more cells with orange and red fluorescence were observed. As the laser power reached 1.5 W cm^{-2}, most of cells showed red and orange fluorescence. The orange fluorescence of the cells observed from the second group was a result of the overlapping of the red fluorescence from the PI and the green fluorescence from the calcein AM, as PI entered the cell through the membrane of the dead cell before the calcein AM completely drained from the cell.[26,27] The emergence of the orange and red fluorescence with the increase of the laser power suggested that the cells in the second group were indeed damaged by the laser. These results demonstrated that the AuNBPs-mPEG/AA-TR has a favorable PTT ability for the CCRF-CEM cells.
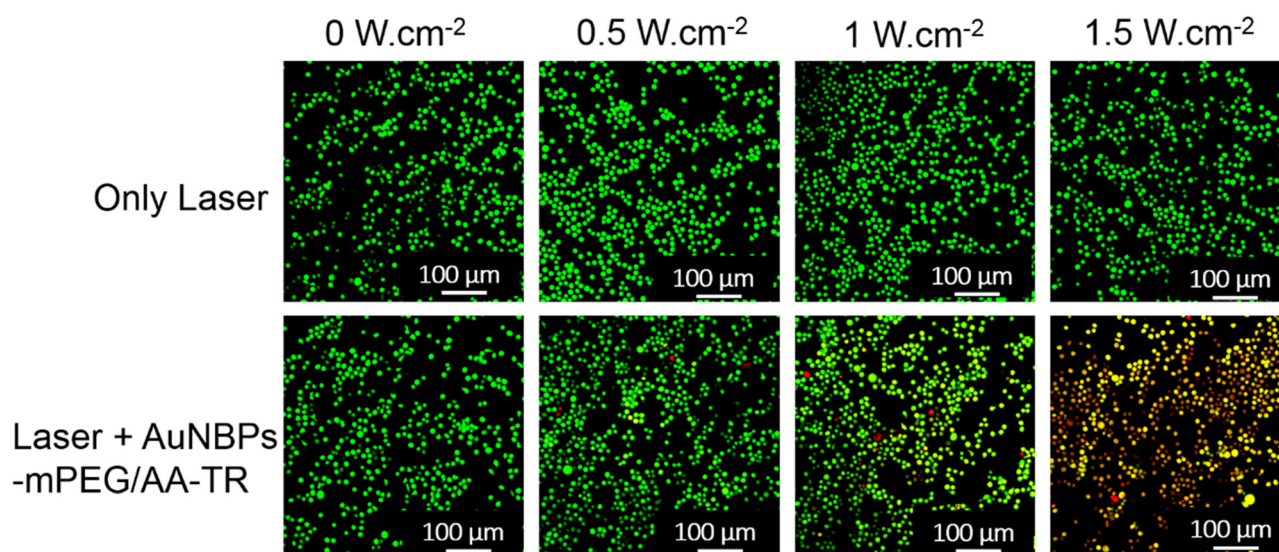

Fig. 7 Survival status of the CCRF-CEM cells exposed to different powers of the laser (808 nm, 0, 0.5, 1, 1.5 W cm^{-2}) for 10 minutes with or without incubation of AuNBPs-mPEG/AA-TR.

Conclusions

In conclusion, AuNBPs-mPEG/AA-TR, a multifunction photo-thermal reagent, was successfully fabricated. Experimental results from flow cytometry analysis and the fluorescence confocal microscopy image verified that the reagent can actively anchor to CCRF-CEM cells through the interaction between the aptamer sgc8 sequence and PTK7 protein on the cell surface. Data from the fluorescence spectra analysis indicated that the fluorescence intensity was doubled when AuNBPs-mPEG/AA-TR binds to the CCRF-CEM cells, manifesting the activatable fluorescence function of the reagent. Meanwhile, a live/dead cell assay proved that the AuNBPs-mPEG/AA-TR had an excellent PPT ability toward CCRF-CEM cells. This multifunctional reagent present in this work has the potential to improve the therapeutic effect of photothermal therapy by means of targeting and activatable fluorescence function, enabling the clinicians to clearly differentiate between normal and cancerous cells.

Author contributions

L. X. Mu and W. S. Shi designed the experiments; X. K. Wu and C. Y. Yan performed the research; C. Y. Yan, Y. Wang and G. W. She contributed to data analysis; X. K. Wu and L. X. Mu wrote the manuscript with help from W. S. Shi. All the authors read and approved the final manuscript.

Conflicts of interest

There are no conflicts to declare.

Acknowledgements

References

1 S. Lal, S. E. Clare and N. J. Halas, *Acc. Chem. Res.*, 2008, **41**, 1842–1851.

2 L. Cheng, C. Wang, L. Feng, K. Yang and Z. Liu, *Chem. Rev.*, 2014, **114**, 10869–10939.

3 S. M. Amini, *J. Therm. Biol.*, 2019, **79**, 81–84.

4 Q. Ni, Z. Teng, M. Dang, Y. Tian, Y. Zhang, P. Huang, X. Su, N. Lu, Z. Yang, W. Tian, S. Wang, W. Liu, Y. Tang, G. Lu and L. Zhang, *Nanoscale*, 2017, **9**, 1466–1474.

5 F. X. Zhao, X. Li, J. Li, Y. Dou, L. W. Wang, M. L. Wu, Y. J. Liu, J. Chang and X. N. Zhang, *J. Mater. Chem. B*, 2017, **5**, 2145–2151.

6 S. Y. Lee, Y. Han, J. W. Hong and J. W. Ha, *Nanoscale*, 2017, **9**, 12060–12067.

7 X. K. Wu, L. X. Mu, M. Chen, S. Liang, Y. Wang, G. W. She and W. S. Shi, *ACS Appl. Biomater.*, 2019, **2**, 2668–2675.

8 B. Liu, F. Q. Jiang, J. Sun, F. Wang and K. Liu, *J. Mater. Chem. B*, 2021, **9**, 7007–7022.

9 S. Lee, P. Kumar, Y. Hu, G. J. Cheng and J. Irudayaraj, *Chem. Commun.*, 2015, **51**, 15494.

10 J. Feng, L. Chen, Y. Xia, J. Xing, Z. Li, Q. Qian, Y. Wang, A. Wu, L. Zeng and Y. Zhou, *ACS Biomater. Sci. Eng.*, 2017, **3**, 608–618.

11 Y. Cao, S. H. Han, H. Zhang, J. Wang, Q. Y. Jiang, Y. Zhou, Y. J. Yu, J. F. Wang, F. Chen and D. K. P. Ng, *J. Mater. Chem. B*, 2021, **9**, 5780–5784.

12 J. Wang, H. Zhang, X. Xiao, D. Liang, X. Y. Liang, L. Mi, J. F. Wang and J. Liu, *Acta Biomater.*, 2020, **107**, 260–271.

13 Y. H. Liu, Z. W. Li, Z. B. Yin, H. X. Zhang, Y. Gao, G. Y. Huo, A. G. Wu and L. Y. Zeng, *ACS Appl. Mater. Interfaces*, 2020, **12**, 14866–14875.

14 X. Song, Q. Chen and Z. Liu, *Nano Res.*, 2015, **8**, 340–354.

15 Z. M. Markovic, L. M. Harhaji-Trajkovic, B. M. Todorovic-Markovic, D. P. Kepic, K. M. Arsikin, S. P. Jovanovic, A. C. Pantovic, M. D. Dramicanin and V. S. Trajkovic, *Biomaterials*, 2011, **32**, 1121–1129.

16 R. Ahmad, J. Fu, N. He and S. Li, *J. Nanosci. Nanotechnol.*, 2016, **16**, 67–80.

17 H. Kobayashi, R. Watanabe and P. L. Choyke, *Theranostics*, 2014, **4**, 81–89.

18 H. M. Meng, H. Liu, H. Kuai, R. Peng, L. Mo and X. B. Zhang, *Chem. Soc. Rev.*, 2016, **45**, 2583–2602.

19 S. Zong, L. Wang, Z. Yang, H. Wang, Z. Wang and Y. Cui, *ACS Appl. Mater. Interfaces*, 2019, **11**, 896–5902.

20 J. Wang, G. Zhu, M. You, E. Song, M. I. Shukoor, K. Zhang, M. B. Altman, Y. Chen, Z. Zhu, C. Z. Huang and W. Tan, *ACS Nano*, 2012, **6**, 5070–5077.

21 Y. Yang, J. Liu, X. Sun, L. Feng, W. Zhu, Z. Liu and M. Chen, *Nano Res.*, 2016, **9**, 139–148.

22 S. Zong, L. Wang, Z. Yang, H. Wang, Z. Wang and Y. Cui, *ACS Appl. Mater. Interfaces*, 2019, **11**, 5896–5902.

23 G. Zhu and X. Chen, *Adv. Drug Delivery Rev.*, 2019, **134**, 65–78.

24 H. Shi, Y. Lei, J. Ge, X. He, W. Cui, X. Ye, J. Liu and K. Wang, *Anal. Chem.*, 2019, **91**, 9154–9160.

25 H. Shi, X. He, K. Wang, X. Wu, X. Ye, Q. Guo, W. Tan, Z. Qing, X. Yang and B. Zhou, *Proc. Natl. Acad. Sci. U. S. A.*, 2011, **108**, 3900–3905.

26 C. X. Li, E. Mei, C. G. Chen, Y. S. Li, B. Nugasur, L. Y. Hou, X. X. Ding, M. R. Hu, Y. F. Zhang, Z. Q. Su, J. Lin, Y. Yang, P. Huang and Z. M. Li, *ACS Appl. Mater. Interfaces*, 2020, **12**, 12541–12548.

27 Y. F. Kang, B. Zheng, C. Y. Li, Z. L. Zhang, H. W. Tang, Q. S. Wu and D. W. Pang, *Anal. Chem.*, 2020, **92**, 1292–1300.